Theoretical hole mobility in a narrow Si/SiGe quantum well

B. Laikhtman
Racah Institute of Physics, Hebrew University, Jerusalem 91904, Israel

R. A. Kiehl*
IBM Research Division, Thomas J. Watson Research Center, Yorktown Heights, New York 10598
(Received 16 November 1992)

Calculations of the hole mobility in a strained SiGe quantum well on (001) Si are carried out for the case of a narrow well in which the subband splittings are large due to quantum-size effects. An envelope-function model for the valence-band structure and hole wave functions in an infinite square well and calculations of scattering rates in a single parabolic band with an isotropic effective mass are used to delineate limitations on mobility imposed by lattice scattering, background impurities, alloy scattering, and interface roughness. Additional scattering mechanisms associated with compositional fluctuations in the SiGe layer are also discussed. Narrow wells (60 Å) with high Ge content (40%) have large subband splittings and exhibit a light mass for hole densities well beyond 10^{12} cm^{-2}. Scattering rates in such structures are greatly reduced as a result of the light mass and large subband splittings. Numerical results indicate that hole mobilities in the mid 10^3 cm^2/V s at room temperature and in the mid 10^4 cm^2/V s at low temperature could be possible in narrow SiGe wells as a result of the favorable modifications in band structure and scattering.

I. INTRODUCTION

The recent interest in Si/SiGe heterostructures for *p*-channel metal-oxide-semiconductor field-effect transistors (MOSFET's) has been primarily motivated by the potential for lower interface-roughness scattering and the reduction of hole mass due to strain.[1,2] Reduced interface-roughness scattering is expected from the isolation of the holes from the rough SiO_2/Si interface by confinement within the SiGe layer, while a light in-plane mass is expected from the splitting of the light- and heavy-hole bands by the biaxial compressive strain in a SiGe layer on (001) Si,[4] similar to the case in GaAs/$In_xGa_{1-x}As$ and other III-V materials.[5] While experimental results are limited, measurements of hole mobility in Si/SiGe heterostructures[6,7] and preliminary results on short-channel Si/SiGe MOSFET's (Refs. 8 and 9) indicate that some advantage can be gained in such structures. The work reported thus far has typically focused on SiGe layers with Ge contents of about 20% and thicknesses of 100 Å or more.

In addition to the reduction of roughness scattering and the strain-induced band splitting, several other effects could be useful for obtaining enhanced hole transport in a Si/SiGe heterostructure. Quantum-size effects (QSE) provide a means for increasing the subband splitting beyond that possible with strain alone, provided that the well is sufficiently deep as in the case of an $Al_yGa_{1-y}As/In_xGa_{1-x}As$ heterostructure.[10,11] Thus, narrow SiGe wells with high Ge content should allow a light mass to be maintained at high hole densities and high temperatures. The light-hole mass and large subband splitting in a narrow quantum well would also result in a reduced phase space for scattering. Scattering rates for all scattering processes therefore should be reduced. These effects would allow the design of a narrow SiGe quantum well having more favorable band structure and reduced scattering, thereby providing a significantly enhanced hole mobility. In this paper, we present theoretical estimates of the limits of the mobility in such heterostructures.

The degeneracy of the hole band structure leads to a complicated coupling of holes with phonons[12] and makes the mobility calculation for holes more difficult than for electrons. In earlier works on mobility calculation in bulk material[13–16] and in accumulation layers,[17] these complications were avoided by the introduction of an electronlike coupling with an effective deformation potential. Tiersten[18] obtained a rather complicated analytic expression for bulk mobility limited by deformation-potential interaction with acoustic phonons. Szmulowicz[19] carried out detailed numerical mobility calculations for bulk Si and Ge using the $\mathbf{k}\cdot\mathbf{p}$ method with 6×6 Kane's Hamiltonian. Hinckley and Singh[4] made Monte Carlo calculations for a SiGe bulk alloy under strain, taking into account light and heavy holes and the spin-orbit split band. The same kind of approach was used by Kelsall *et al.*[20,21] for AlAs/GaAs and GaAs/$In_xGa_{1-x}As$ quantum wells.

Here, we consider SiGe wells pseudomorphically strained to match a (001) Si substrate. We take advantage of the quantum-size effect and limit ourselves to the extreme case where the splittings of the heavy-hole subbands HH*n* and the light-hole subbands LH*n* are large compared to all other characteristic energies, such as the Fermi energy and temperature. We use an envelope-function model to determine the valence-band structure in a strained SiGe quantum well. The large subband splitting in a narrow well allows us to consider transport by scattering in the highest subband only. The theory of hole transport in this case is similar to that for electrons,

which has been treated by Gold[22] for a SiGe quantum well within the envelope-function approximation. The previous work by Gold considers only very low temperatures, however, while we are interested mainly in temperatures of 77 K and higher. At the same time we will make use of some of the analytic results obtained by Gold,[22] and the results of our calculations for background scattering and surface-roughness scattering can be compared with those for electrons by scaling the effective mass. There is an important difference between the present case and the case of a simple band structure. The difference concerns the hole wave functions and Hamiltonians coupling holes with scatterers. In particular, there is a selection rule forbidding the deformation-potential scattering by optical phonons in a simple band.[11] The large splitting, however, allows a small admixture of upper subbands at finite wave vectors **k** which makes the optical deformation-potential scattering possible. In our calculations we consider this admixture as a small correction to the wave function which simplifies the calculation of the scattering matrix element. For other scattering mechanisms where there is no such selection rule, we neglect the admixture.

In the next section we consider the band structure of a narrow SiGe quantum well. We show the effect of strain and size quantization on the masses and subband splittings. We also show that the nonparabolicity and anisotropy of the highest subband (HH1) are small and can be neglected for narrow wells with high Ge content. In Sec. III, the scattering matrix elements and scattering rates which we use in the numerical calculations are given. These include single-band models for conventional mechanisms such as optical and acoustic phonons, which usually dominate at high temperatures, and for scattering by structural imperfections like alloy disorder, interface roughness, and ionized impurities. We also consider alloy-assisted optical-phonon scattering which may be important in SiGe because the alloy disorder to some extent lifts the selection rule for the deformation optical-phonon scattering. We neglect the scattering by misfit dislocations assuming that they are avoided in the growth of the structure. In Sec. IV, the scattering by compositional fluctuations is discussed. Fluctuations in the Ge composition along the quantum well result in strain fluctuations, and the scattering by these strain fluctuations could be very important because of the large value of the deformation potential. In Sec. V, results of the numerical calculation of the mobility are presented. The mobility limits imposed by the various mechanisms are considered separately for different parameter values. Finally, the conclusions are given in Sec. VI.

II. BAND STRUCTURE

The band-structure model used in the calculations was originally developed for the case of a strained $Al_yGa_{1-y}As/In_xGa_{1-x}As$ quantum well and has been described in detail elsewhere.[23] It is based on an envelope-function formulation for the valence band in a strained, infinite square well. The assumption of an infinite square well is justified in the case of a high Ge content due to the very large valence-band offset at the $Si_{1-x}Ge_x/Si$ interface, which is $0.74x$ eV.[24–26] For a 60-Å well with $x=0.4$, for example, the band offset is 300 meV and the HH1 level is 40 meV from the bottom of the well, so that the actual barrier for holes in this subband is 260 meV. This barrier is much larger than the typical Fermi energy (6 meV for the concentration of 1×10^{12} cm^{-2}) and the thermal energy (25 meV at 300 K). The hole wave function falls off exponentially in such a barrier over a characteristic distance about 6 Å (in this estimate we used a hole effective mass of 0.4 for Si). One effect of the finite barrier penetration is to reduce the difference between the HH1 subband and the bottom of the well, i.e., to increase the barrier height. In addition, the above estimates assume that the interface is a potential barrier with a height equal to the band offset. Actually the boundary conditions at the interface are more complicated,[27] and this improves the hole confinement in the quantum well.

The penetration of the wave function under the barrier leads to corrections in the scattering matrix elements used in the mobility calculations, which are evaluated using the wave functions for an infinite well. This correction is small, however, since the penetration distance is much smaller than the width of the well and the distortion of the wave function is therefore negligible. The penetration also leads to a reduction in the self-consistent field for carriers inside the well. The effective potential associated with this field is only about 10 meV for a hole density of 1×10^{12} cm^{-2}, however, which is much smaller than all energies determining the shape of the wave function in the well. Hence, the self-consistent field can be neglected.

We also neglect the spin-orbit split subband. While the splitting of the spin-orbit band is small (40 meV) in the case of Si, the splitting is reasonably large in SiGe alloys with high Ge content (e.g., 300 meV in pure Ge). Moreover, the splitting increases very rapidly in a narrow well due to the light mass of this band. Hence, this is a good assumption in the case of the narrow, high Ge content wells of interest here. Following what has commonly been done in calculations for SiGe alloys, the values of the constants were obtained by linear interpolation from values in Si and Ge. These values are given in Table I.

Figure 1 shows the calculated band structure for an 80-Å well with 15% Ge, which represents a relatively wide well and a low Ge content. (Higher-order subbands are included for completeness of the solutions for an infinite well, although the dispersion law for a real structure would be substantially changed at energies near the barrier height for the well.) The top of the HH band is taken as the zero-energy reference in the figure and the top of the strain-split LH band is indicated by the dot-dash line. Solid and dashed curves represent the (100) and (110) directions, respectively. We plot the electron energy versus $k_{\parallel}^2$, the square of the in-plane wave vector. Hence, the x axis is proportional to hole density while the slopes in the curves are inversely proportional to the in-plane masses. It is seen that the subbands are highly nonparabolic except for the HH1 subband, which is parabolic over a relatively large range of $k_{\parallel}^2$ and exhibits a light-

TABLE I. Si and Ge lattice constants, inverse-mass band parameters (A, B, and C), hydrostatic deformation potentials (a), shear deformation potentials (b), optical-phonon energies ($\hbar\omega$), relative dielectric constants (κ), optical deformation potentials (d_0), and elastic moduli (c_{11} and c_{12}) used in the calculations. Values are taken from Ref. 28, except for d_0 which is taken from Ref. 19. Due to an elastic anisotropy, average values were used for c_{11} and c_{12}.

	Lattice const. (Å)	Band parameters ($\hbar^2/2m_0$)			Deformation potentials (eV)		$\hbar\omega$ (meV)	d_0 (eV)	κ	Elastic moduli (10^{11} dyn cm^{-2})	
		A	B	C	a	b				c_{11}	c_{12}
Si	5.43	4.27	0.63	4.93	−10.2	2.2	63	29.3	11.9	16.58	6.39
Ge	5.65	13.3	8.57	12.78	−12.4	2.2	37	40	16.0	12.00	6.13

hole mass of about 0.18 over this range. The bands are isotropic near $k_{\|}^2=0$ but become anisotropic at large wave vectors. It may also be noted that the slope is positive for the HH2 subband near $k_{\|}^2=0$, representing an electronlike mass. The QSE-induced splitting of the HH1 and HH2 subbands is 65 meV, which is comparable to the 48-meV strain-induced splitting of the HH and LH bands. The combination of strain and QSE results in a 70-meV splitting between HH1 and LH1, the highest LH subband.

Although the ground-state mass is light near $k_{\|}^2=0$ in the 80-Å, 15% well, the splitting between this band and the HH2 band, which has a very heavy mass, is too small to permit a light mass to be maintained at high hole densities. A sheet density of 5×10^{12} cm^{-2}, for example, which is typical of that in a fully accumulated field-effect transitor (FET) channel, corresponds to $k_{\|}^2=0.3$ nm^{-2}. It is clear from Fig. 1 that a significant population of the heavy HH2 band would occur for wave vectors in this range.

An increased Ge content is favorable to the band structure for several reasons. A higher Ge content results in lighter HH- and LH-band masses, in a larger ratio of these masses, and in a greater strain-induced band splitting. Because of the lighter HH- and LH-band masses, the QSE-induced subband splitting also increases with Ge content. In addition to these factors, a larger Ge content is favorable since it results in a deeper well. A deep well is required to exploit QSE since it allows large subband splittings. The depth of a 15% Ge well, for example, is only 110 meV, which limits the actual subband splittings to even smaller values than those calculated for the infinite well in Fig. 1.

Figure 2 shows the effect of increasing the Ge content in the well. The figure shows results for a 45% well with the same 80-Å thickness as Fig. 1. The HH1 mass in this case is reduced to 0.11 at $k_{\|}^2=0$ and light mass persists to larger values of $k_{\|}^2$. The HH1-HH2 and HH1-LH1 splittings increase to 72 and 190 meV, respectively. Although the LH1 band is now pushed far below the ground state and is essentially out of the picture, the accumulation of a high hole density would again involve a heavy population of the HH2 band, which has a heavy mass of 0.30 in this case.

It is apparent that larger subband splittings than those in Fig. 2 are needed to provide light mass at high densities or high temperatures. Improvement by further increases in the Ge content is not possible due to critical thickness limitations on the layer strain. (According to the single-kink dislocation model,[29] the 45% Ge content is, in fact, already higher than the 32% thermodynamic stability limit for an 80-Å SiGe layer.) Increased subband splitting can be obtained, however, by narrowing the

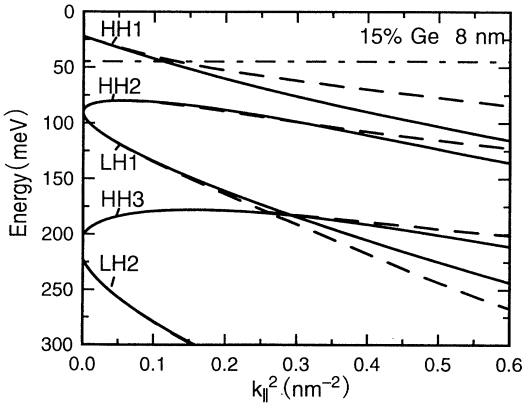

FIG. 1. Band structure for an 80-Å, 15% Ge well in the (100) direction (solid curves) and (110) direction (dashed curves). Zero energy is referenced to the HH band edge. The strain-split LH band edge is indicated by the dash-dotted line.

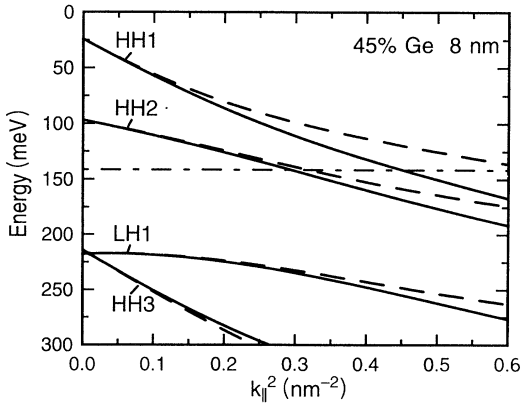

FIG. 2. Band structure for an 80-Å, 45% Ge well.

well.

Figure 3 shows the effect of decreasing the well thickness to 45 Å. Narrowing the well is seen to have little effect on the HH1 subband, except for a shift in energy. Despite this shift, this subband remains highly confined within the 330-meV deep well (45% Ge). The HH2 subband is pushed down in energy, resulting in a HH1-HH2 splitting of 230 meV. Population of the HH1 subband to a density of 5×10^{12} cm^{-2}, corresponding to $k_{\parallel}^2=0.3$ nm^{-2}, can now be attained with negligible population of the HH2 subband, which is many kT away even at room temperature.

The main features of the band-structure calculations which are important for the calculation of the mobility are (i) the large separation of the uppermost subbands and (ii) the small deviation of the hole spectrum from a parabolic shape. The first point allows us to neglect intersubband scattering and the second point allows us to use a simple isotropic spectrum for the HH1 subband.

For the calculation of the scattering matrix element we need the hole envelope wave functions. In the basis of light and heavy holes they have the form

$$\psi_{\text{even}}(\mathbf{r},z)=\begin{bmatrix}\psi_{e1}(z)\\ \psi_{e2}(z)\\ \psi_{e3}(z)\\ \psi_{e4}(z)\end{bmatrix}\frac{1}{\sqrt{S}}e^{i\mathbf{kr}}\ ,$$
$$\psi_{\text{odd}}(\mathbf{r},z)=\begin{bmatrix}\psi_{o1}(z)\\ \psi_{o2}(z)\\ \psi_{o3}(z)\\ \psi_{o4}(z)\end{bmatrix}\frac{1}{\sqrt{S}}e^{i\mathbf{kr}}\ , \tag{1}$$

where $\mathbf{r}$ and z are coordinates in plane and in the direction perpendicular to the quantum well, respectively, $\mathbf{k}$ is the in-plane wave vector, and S is the normalization area. The exact forms of the components ψ_{ej} and ψ_{oj} are rather complicated even in the model of the infinite square well.[23] However, for the mobility calculation we only need wave functions near the top of the HH1 subband. In the first approximation we can take

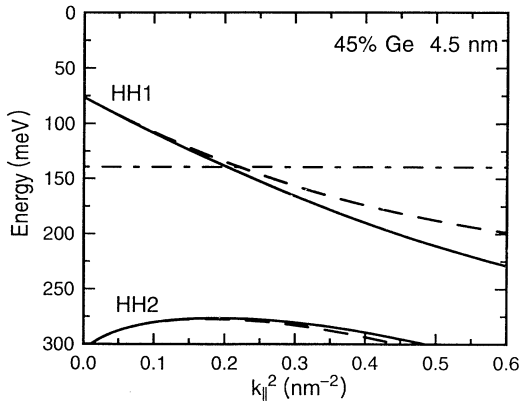

FIG. 3. Band structure for a 40-Å, 45% Ge well.

$$\psi_{e1}(z)=\psi_{o4}(z)=\left[\frac{2}{L}\right]^{1/2}\cos\frac{\pi z}{L} \tag{2}$$

and neglect all others. In this approximation there is no scattering between the even and odd states, and it is sufficient to consider either one of them. For optical-phonon scattering such an approximation gives a zero result.[11] In this case we will use the next approximation (see Sec. III E).

III. CONVENTIONAL SCATTERING MECHANISMS

The results of the band-structure calculation show that for a quantum well with a width smaller than 80 Å the separation between the highest subband HH1 and the next subband HH2 is larger than 50 meV. Since the Fermi energy for the concentration 10^{12} cm^{-2} is about 10 meV and the thermal energy at room temperature is 25 meV, nearly all carriers are in the HH1 subband at room temperature and below. Therefore, we deal with essentially one subband transport. The results of Sec. II show that the HH1 subband is nearly parabolic and isotropic. If we also neglect an anisotropy of scattering (e.g., an elastic anisotropy) we can use the relaxation-time approximation which makes a major simplification of the mobility calculation (compare Ref. 19).

The solution of the Boltzmann equation for an elastic scattering leads to the following expression for the inverse transport relaxation time:

$$\frac{1}{\tau}=-\frac{2\pi}{\hbar k}\int\frac{|M_q|^2 q\cos\phi}{\left\{1+\frac{q_s}{q}H(q)\Pi(0,q)\right\}^2}\times\delta(E_{\mathbf{k}+\mathbf{q}}-E_k)\frac{d^2\mathbf{q}}{(2\pi)^2}\ . \tag{3}$$

Here E_k is the energy of a carrier with the wave vector $\mathbf{k}$, $\mathbf{q}$ is the wave vector transferred in a scattering event, M_q is a scattering matrix element, and ϕ is the angle between $\mathbf{k}$ and $\mathbf{q}$. The static dielectric function $\epsilon(0,q)$ in the integrand in Eq. (3) results from the screening of the scattering potential by two-dimensional (2D) gas. The calculation of $\epsilon(0,q)$ is reduced to the solution of electrostatic equations in the quantum well and the substrate. The result is expressed in terms of the dimensionless polarization operator $\Pi(0,q)$ and the scattering matrix element $H(q)$ (see e.g., Ref. 30),

$$\epsilon(0,q)=1+\frac{q_s}{q}H(q)\Pi(0,q)\ . \tag{4}$$

Here $q_s=2me^2/\kappa_1\hbar^2$ is the screening parameter, e is the electron charge, and κ_0 and κ_1 are dielectric constants in the substrate and in the quantum well, respectively. The polarization operator describes the response of the 2D gas on an external perturbation,[30] and the screening matrix element is a form factor depending on the wave functions and electric-field distribution. For a square infinite quantum well it has the form

$$H(q)=\frac{(\kappa_0+\kappa_1)^2}{(\kappa_0+\kappa_1)^2-(\kappa_0-\kappa_1)^2e^{-2qL}}\left[\frac{2}{L}\right]^2 \times\int_{-L/2}^{L/2}F_s(z,z')\cos^2\frac{\pi z}{L}\cos^2\frac{\pi z'}{L}dz\,dz' , \quad (5)$$

where

$$F_s(z,z')=e^{-q|z-z'|}-2\frac{\kappa_0-\kappa_1}{\kappa_0+\kappa_1}e^{-qL}\cosh q(z+z') + \left[\frac{\kappa_0-\kappa_1}{\kappa_0+\kappa_1}\right]^2 e^{-2qL+q|z-z'|} \quad (6)$$

[compare Eqs. (2.51) and (2.52) in Ref. 30 for an inversion layer]. In the case of $\kappa_0=\kappa_1$ the matrix element takes the form[31]

$$H(q)=\frac{2}{qL}+\frac{qL}{(qL)^2+4\pi^2} -\frac{32\pi^4}{(qL)^2[(qL)^2+4\pi^2]^2}(1-e^{-qL}) . \quad (7)$$

The dimensionless polarization operator for zero transferred energy (i.e., omitting all dynamic effects) (Refs. 30 and 32) can be reduced to

$$\Pi(0,q)=\int_0^1\frac{dx}{\exp\left[\frac{E_q}{4k_BT}(1-x^2)-\frac{\zeta}{k_BT}\right]+1} . \quad (8)$$

Here the chemical potential ζ is connected with the concentration n and the Fermi energy $E_F\equiv\zeta|_{T=0}=\pi\hbar^2n/m$ by the relation

$$\exp\left[\frac{E_F}{k_BT}\right]=1+\exp\left[\frac{\zeta}{k_BT}\right] . \quad (9)$$

Both E_F and ζ refer to hole (not electron) energies and are measured from the HH1 band edge. Equation (8) can be simplified in the case of low and high temperatures,

$$\Pi(0,q)=1 , \quad k_BT\ll E_F , \quad (10)$$

$$\Pi(0,q)=\frac{E_F}{k_BT}\int_0^1 e^{-(E_q/4k_BT)(1-x^2)}dx , \quad k_BT\gg E_F . \quad (11)$$

The integration with respect to ϕ in Eq. (3) reduces it to a simpler form,[22,31]

$$\frac{1}{\tau}=\frac{m}{\pi\hbar^3k^2}\int_0^{2k}\frac{|M_q|^2}{\left\{1+\frac{q_s}{q}H(q)\Pi(0,q)\right\}^2}\frac{q^2dq}{(4k^2-q^2)^{1/2}} . \quad (12)$$

It is worth noting that Eq. (12) is simplified at sufficiently high temperatures, when $q_sE_F/k_BT\ll q$, the screening can be neglected.

The mobility is expressed as

$$\mu=\frac{e}{4\pi\hbar^2nk_BT}\int_0^\infty\frac{E\tau(E)dE}{\cosh^2\left[\frac{E-\zeta}{2k_BT}\right]} . \quad (13)$$

In the cases of low and high temperature Eq. (13) can be reduced to

$$\mu=\frac{e\tau(E_F)}{m} , \quad k_BT\ll E_F , \quad (14)$$

$$\mu=\frac{e}{m(k_BT)^2}\int_0^\infty E\tau(E)e^{-E/k_BT}dE , \quad k_BT\gg E_F . \quad (15)$$

In the remainder of this section we review the relevant expressions for scattering matrix elements for different scattering mechanisms and also derive expressions for the relaxation time for inelastic processes involving optical phonons.

A. Ionized impurity scattering

For Coulomb scattering the matrix element is

$$|M_q|^2=\left[\frac{2\pi e^2}{\kappa_0q}\right]^2\int N_I(z)[F_I(q,z)]^2dz . \quad (16)$$

$N_I(z)$ is the impurity concentration, and the form factor is

$$F_I(q,z)=\frac{(\kappa_0+\kappa_1)^2}{(\kappa_0+\kappa_1)^2-(\kappa_0-\kappa_1)^2e^{-2qL}} \times\frac{2}{L}\int_{-L/2}^{L/2}\tilde{F}_I(z,z')\cos^2\frac{\pi z'}{L}dz' , \quad (17)$$

where $\tilde{F}_I(z,z')$ is the Fourier component of the field created by a point charge near a quantum well. As well as $H(q)$ it is determined from the solution of the electrostatic equation in the quantum well and substrate. The result is

$$\tilde{F}_I(z,z')=\frac{2\kappa_0}{\kappa_0+\kappa_1}\left[e^{-q|z-z'|}-\frac{\kappa_0-\kappa_1}{\kappa_0+\kappa_1}e^{-q|z+z'|-qL}\right] , \quad |z|>\frac{L}{2} , \quad (18)$$

$$\tilde{F}_I(z,z')=-\frac{\kappa_0}{\kappa_1}F_s(z,z') , \quad |z|<\frac{L}{2} . \quad (19)$$

In the case of $\kappa_0=\kappa_1$,

$$F_I(q,z)=\frac{2}{L}\int_{-L/2}^{L/2}e^{-q|z-z'|}\cos^2\frac{\pi z'}{L}dz' . \quad (20)$$

For a uniform background scattering

$$|M_q|^2=\left[\frac{2\pi e^2}{\kappa q}\right]^2N_ILF_B(qL) , \quad (21)$$

where

$$F_B(x)=\frac{4}{x^2}+\frac{2x^2}{(x^2+4\pi^2)^2}-\frac{96\pi^4}{x^3(x^2+4\pi^2)^2}(1-e^{-x}) -\frac{128\pi^4}{x(x^2+4\pi^2)^3}(1-e^{-x})+\frac{32\pi^4}{x^2(x^2+4\pi^2)^2}e^{-x} . \tag{22}$$

B. Interface-roughness scattering

The interface roughness in quantum wells is usually considered as a random modulation of the width of the quantum well $\Delta(\mathbf{r})$, which changes the position of the subband levels.[22,33,34] The roughness is characterized by two parameters, the average height Δ and the correlation length Λ. Such an approach is justified only if Δ is much smaller than the width of the well while Λ is much larger than the width. For Δ, this condition is necessary to justify the Born approximation in the calculation of scattering. If Λ violates this condition, then the wave functions in the well are distorted and the effective potential is different from the adiabatic modulation of energy levels. In practical applications the latter complication may not be important because two adjustable parameters leave enough freedom to approximate another scattering potential.

For the Gaussian distribution function of the roughness

$$\langle \Delta(\mathbf{r})\Delta(\mathbf{r}')\rangle=\Delta^2\exp\left[-\frac{(\mathbf{r}-\mathbf{r}')^2}{\Lambda^2}\right] , \tag{23}$$

the averaged scattering matrix element is[22,33–35]

$$|M_q|^2=\frac{\pi^5\hbar^4\Delta^2\Lambda^2}{m_z^2L^6}e^{-q^2\Lambda^2/4} , \tag{24}$$

where the effective mass of the HH1 subband in the z direction is determined by the expression

$$\frac{\hbar^2}{2m_z}=A-B , \tag{25}$$

and A, B, and C are the inverse-mass band parameters.[36]

In the case of a large correlation length $\Lambda\gg L,\hbar/\sqrt{8mk_BT}$, the main contribution to the integral in Eq. (12) comes from a region of q so small that the relaxation rate due to the interface-roughness scattering can be reduced to a simpler form. In this case $H(q)=1$, $\Pi(0,q)=1-\exp(-E_F/k_BT)$, and

$$\frac{1}{\tau_{\rm rgh}}=\frac{\pi^4\hbar\Delta^2\Lambda^2m}{2m_z^2L^6k^3}\int_0^\infty e^{-q^2\Lambda^2/4} \times\frac{q^4dq}{\{q+q_s[1-\exp(-E_F/k_BT)]\}^2} . \tag{26}$$

A further simplification is possible for low temperatures when q in the integrand can be neglected compared to q_s which is typically about k_F,

$$\frac{1}{\tau_{\rm rgh}}=\frac{6\pi^{9/2}\hbar\Delta^2m}{m_z^2L^6q_s^2\Lambda^3k^3} , \quad k_BT\ll E_F . \tag{27}$$

The physical reason for the resulting dependence of the scattering rate on Λ and k is easy to understand. With the increase of the product Λk carriers "see" a smoother interface and the scattering drops.

Making use of Eqs. (27) and (14) we can get a simple expression for the interface-roughness limited mobility at low temperatures,

$$\mu_{\rm rgh}=\frac{2^{1/2}em_z^2L^6q_s^2\Lambda^3n^{3/2}}{3\pi^3\hbar\Delta^2m^2} , \quad k_BT\ll E_F . \tag{28}$$

Another simple expression for $\mu_{\rm rgh}$ can be obtained in the case of high temperatures such that $\Lambda q_sE_F/k_BT\ll1$ and the screening in Eq. (26) can be neglected. Then

$$\frac{1}{\tau_{\rm rgh}}=\frac{\pi^{9/2}\hbar\Delta^2m}{m_z^2L^6\Lambda k^3} , \tag{29}$$

and Eq. (15) gives

$$\mu_{\rm rgh}=\frac{15em_z^2L^6\Lambda(k_BT)^{3/2}}{2^{3/2}\pi^4\hbar^4\Delta^2m^{1/2}} . \tag{30}$$

C. Alloy scattering

For alloy scattering in a $Si_{1-x}Ge_x$ alloy we use the scattering potential

$$U_{\rm al}(\mathbf{r})=\tfrac{1}{2}u_{\rm al}a_0^3\sum_j\delta(\mathbf{r}-\mathbf{r}_j) , \tag{31}$$

where $u_{\rm al}$ is the energy associated with an alloy atom, a_0 is the lattice constant, $\mathbf{r}_j$ are positions of alloy atoms, and the factor $\frac{1}{2}$ corresponds to two atoms in a unit cell.[37–39] Equation (31) gives

$$|M_q|^2=\frac{3u_{\rm al}^2a_0^3x(1-x)}{4L} . \tag{32}$$

D. Acoustic-phonon scattering

The deformation-potential Hamiltonian for the coupling between acoustic phonons and holes has the form[12]

$$\mathcal{H}_{\rm ph}=\begin{bmatrix} f & h & j & 0\\ h^* & g & 0 & j\\ j^* & 0 & g & -h\\ 0 & j^* & -h^* & 0\end{bmatrix} , \tag{33}$$

where

$$f=a(u_{xx}+u_{yy}+u_{zz})+b\left[\frac{u_{xx}+u_{yy}}{2}-u_{zz}\right] , \tag{34}$$

$$g=a(u_{xx}+u_{yy}+u_{zz})-b\left[\frac{u_{xx}+u_{yy}}{2}-u_{zz}\right] , \tag{35}$$

$$n=-d(iu_{xz}+u_{yz}) , \tag{36}$$

$$j=\frac{\sqrt{3}}{2}b(u_{xx}-u_{yy})-idu_{xy} , \tag{37}$$

and a, b, and d are deformation potentials. Making use of the wave functions Eq. (1) we get the following expression for the matrix element squared for emission or absorption of a phonon with the polarization s and wave vector $(\mathbf{q},\mathbf{q}_z)$:

$$|\tilde{M}_s(\mathbf{q},q_z)|^2=\frac{\hbar k_B T}{2\rho u_s^2(q^2+q_z^2)}\frac{\pi^4\sin^2(q_zL/2)}{(q_zL/2)^2[(q_zL/2)^2-\pi^2]^2}\times\left[\left[a+\frac{b}{2}\right](q_xe_{sz}+q_ye_{sy})+(a-b)q_ze_{sz}\right]^2 , \tag{38}$$

where ρ is the density, u_s is the sound velocity, and $\mathbf{e}_s$ is the polarization vector. We assumed that the temperature is so high that phonon occupation numbers $N_s\cong k_BT/u_s(q^2+q_z^2)^{1/2}\gg 1$. For longitudinal and transverse phonons Eq. (38) gives

$$|\tilde{M}_l(\mathbf{q},q_z)|^2=\frac{\hbar k_B T}{2\rho u_l^2(q^2+q_z^2)^2}\frac{\pi^4\sin^2(q_zL/2)}{(q_zL/2)^2[(q_zL/2)^2-\pi^2]^2}\times\left[\left[a+\frac{b}{2}\right]q^2+(a-b)q_z^2\right]^2 , \tag{39}$$

$$\sum_{s=t}|\tilde{M}_s(\mathbf{q},q_z)|^2=\frac{\hbar k_B T}{2\rho u_t^2(q^2+q_z^2)^2}\times\frac{\pi^4\sin^2(q_zL/2)}{(q_zL/2)^2[(q_zL/2)^2-\pi^2]^2}\times\left[\frac{3b}{2}\right]^2q^2q_z^2 , \tag{40}$$

where u_l and u_t are the velocities of the longitudinal and the transverse sound, respectively.

After the integration with respect to q_z, using the approximate envelope wave function of Eq. (2), we obtain

$$|M_q|^2=\frac{\pi k_B T}{\rho L}\left\{\frac{1}{u_l^2}\left[a+\frac{b}{2}\right]^2g_1\left[\frac{qL}{2}\right]+\frac{1}{u_l^2}(a-b)^2g_2\left[\frac{qL}{2}\right]+\left[\frac{2}{u_l^2}\left[a+\frac{b}{2}\right](a-b)+\frac{1}{u_t^2}\left[\frac{3b}{2}\right]^2\right]\times g_3\left[\frac{qL}{2}\right]\right\} , \tag{41}$$

where

$$g_1(z)=\frac{3}{2\pi}-\pi\frac{2z^2+\pi^2}{(z^2+\pi^2)^2}-\pi^3\frac{3z^2+\pi^2}{2z(z^2+\pi^2)^3}(1-e^{-2z}) \tag{42}$$

$$-\frac{\pi^3}{4z(z^2+\pi^2)^2}(1-2ze^{-2z}-e^{-2z}) , \tag{43}$$

$$g_2(z)=\frac{\pi^3}{(z^2+\pi^2)^2}\left[1+\frac{\pi^2-3z^2}{4z(z^2+\pi^2)}(1-e^{-2z})+\tfrac{1}{2}e^{-2z}\right] , \tag{44}$$

$$g_3(z)=\frac{\pi}{(z^2+\pi^2)^2}\left[z^2+\pi^2\frac{5z^2+\pi^2}{4z(z^2+\pi^2)}(1-e^{-2z})-\frac{\pi^2}{2}e^{-2z}\right] . \tag{45}$$

If the deformation potential b is much smaller than a, then Eq. (41) is reduced to

$$|M_q|^2=\frac{3a^2k_BT}{2\rho u_l^2L} . \tag{46}$$

At high temperature, $\Lambda q_sE_F/k_BT\ll 1$, when screening can be neglected the integration in Eq. (12) can be carried out analytically and for the acoustic-phonon relaxation rate we get

$$\frac{1}{\tau_{ac}}=\frac{3ma^2k_BT}{2\rho\hbar^3u_l^2L} . \tag{47}$$

The comparison of this expression with the corresponding expression for a bulk crystal

$$\frac{1}{\tau_{ac}^{3D}}=\frac{ma^2k_BT}{\pi\rho\hbar^3u_l^2}k \tag{48}$$

(Refs. 40 and 41), shows that in the 3D case there is another numerical factor and the factor kL.[42,43]

Equation (47) gives the following expression for the acoustic-phonon limited mobility:

$$\mu_{ac}=\frac{2e\rho\hbar^3u_l^2L}{3m^2a^2k_BT} . \tag{49}$$

E. Optical-phonon scattering

The deformation coupling of holes with optical phonons is described by the Hamiltonian[12]

$$\mathcal{H}_{opt}=\begin{bmatrix}0 & iu_y+u_x & -iu_z & 0\\ -iu_y+u_x & 0 & 0 & -iu_z\\ iu_z & 0 & 0 & -iu_y-u_x\\ 0 & iu_z & iu_y-u_x & 0\end{bmatrix}\frac{d_0\sqrt{3}}{a_0} . \tag{50}$$

Here u_k are components of optical-phonon displacement, d_0 is the optical deformation potential, and a_0 is the lattice constant. It is easy to see that if only components $\psi_{e1}(z)$ and $\psi_{o4}(z)$ are taken into account in the wave functions Eq. (1), then the matrix elements of $\mathcal{H}_{\rm opt}$ equal zero. In the next approximation in the ratio of the characteristic energy to the separation between the HH1 and HH2 subbands it is enough to take into account $\psi_{e2}(z)$ and $\psi_{o3}(z)$. Approximate expressions are obtained by the expansion of the exact expressions[23] in terms of kL. The result is

$$\psi_{e2}(z)=\psi^*_{o3}(z)=\frac{DL(k_x+ik_y)}{2\pi B}\left[\sin\frac{\pi z}{L}-\frac{\sin k_L z}{\sin(k_L L/2)}\right], \tag{51}$$

where $D^2=C^2+3B^2$ and $k_L=(A-B)^{1/2}\pi/(A+B)^{1/2}L$. These wave functions give the following matrix elements for the Hamiltonian corresponding to the emission or absorption of a phonon with the wave vector $\mathbf{q}$:

$$\langle\beta,\mathbf{k}'|\mathcal{H}_{\rm opt}|\alpha,\mathbf{k}\rangle=\frac{1}{\sqrt{V}}M^{\alpha\beta}_{\mathbf{k},\mathbf{k}'}\times\begin{cases}\delta_{\mathbf{k}',\mathbf{k}+\mathbf{q}}N^{1/2}\,,\\ \delta_{\mathbf{k}',\mathbf{k}-\mathbf{q}}(N+1)^{1/2}\,,\end{cases} \tag{52}$$

where V is a normalization volume for phonons, α and β take values e or o for even and odd states, respectively, N are phonon occupation numbers, and

$$M^{ee}_{\mathbf{k},\mathbf{k}'}=-i\left[\frac{6\hbar}{\rho\omega}\right]^{1/2}\frac{DLd_0}{Ba_0}F_{\rm opt}(kL)\times[(e_x+ie_y)(k_x+ik_y)+(e_x-ie_y)(k'_x-ik'_y)]\,, \tag{53}$$

$$M^{oo}_{\mathbf{k},\mathbf{k}'}=i\left[\frac{6\hbar}{\rho\omega}\right]^{1/2}\frac{DLd_0}{Ba_0}F_{\rm opt}(kL)\times[(e_x+ie_y)(k'_x+ik'_y)+(e_x-ie_y)(k_x-ik_y)]\,, \tag{54}$$

$$M^{oe}_{\mathbf{k},\mathbf{k}'}=\left[\frac{6\hbar}{\rho\omega}\right]^{1/2}\frac{DLd_0}{Ba_0}F_{\rm opt}(kL)(k_x+ik_y+k'_x+ik'_y)e_z\,. \tag{55}$$

Here ω and $\mathbf{e}$ are the phonon frequency and polarization vector, respectively. We consider the case of two atoms in a unit cell when there are only three branches of optical-phonon spectrum. The form factor

$$F_{\rm opt}(x)=\frac{1}{x^2-4\pi^2}\sin\frac{x}{2}+\frac{1}{(x^2+k_L^2L^2-\pi^2)^2-4x^2k_L^2L^2}\times\left[2xk_LL\cot\frac{k_LL}{2}\cos\frac{x}{2}+(x^2+k_L^2L^2-\pi^2)\sin\frac{x}{2}\right]. \tag{56}$$

The expressions for hole relaxation rates are

$$\frac{1}{\tau^\alpha_{\rm opt}}=\frac{2\pi}{\hbar}\int\frac{d^2\mathbf{k}'}{(2\pi)^2}\sum_{\beta,s}\int\frac{dq_z}{2\pi}|M^{\alpha\beta}_{\mathbf{k},\mathbf{k}'}|^2(\{(N+1)f_0(E_{k'})+N[1-f_0(E_{k'})]\}\delta(E_{k'}-E_k-\hbar\omega)+\{Nf_0(E_{k'})+(N+1)N[1-f_0(E_{k'})]\}\delta(E_{k'}-E_k+\hbar\omega))\,, \tag{57}$$

where s is the phonon polarization. We consider a nonpolar material and assume that transverse and longitudinal phonons have the same frequency.

Screening of the scattering is determined by the polarization operator $\Pi(\omega,q)$, depending on the optical-phonon frequency ω. Typically, the optical-phonon energy $\hbar\omega$ is much larger than the Fermi energy of the 2D gas. In this case the polarization operator is small and screening can be neglected in Eq. (57).

The relaxation times for even and odd states are identical. The optical-phonon scattering is important only at high temperatures when the 2D gas is nondegenerate. For this case, after the summation with respect to s and integration with respect to q_z, Eq. (57) is reduced to

$$\frac{1}{\tau_{\rm opt}}=\frac{9D^2d_0^2L}{8\pi B^2\rho\omega a_0^2}\Phi_{\rm opt}(k_LL)\times\int\frac{d^2\mathbf{k}'}{(2\pi)^2}(k^2+k'^2)\times[N\delta(E_{k'}-E_k-\hbar\omega)+(N+1)\delta(E_{k'}-E_k+\hbar\omega)]\,, \tag{58}$$

where

$$\Phi_{\rm opt}(z)=1+8z\left[\frac{1}{z^2-\pi^2}-\frac{1}{z^2-9\pi^2}\right]\cot\frac{z}{2}+\left[1+\frac{\pi^2}{z^2-\pi^2}\frac{\sin z}{z}\right]\frac{2}{\sin^2\frac{z}{2}}\ . \tag{59}$$

In spite of its appearance this function does not have singularities, $\Phi_{\rm opt}(0)=(21\pi^2-200)/9\pi^2$, $\Phi_{\rm opt}(\pi+\epsilon)=(\frac{1}{4}-15/8\pi^2)\epsilon^2$ for $\epsilon\ll 1$, and $\Phi_{\rm opt}(3\pi)=5$.

After the integration Eq. (58) gives

$$\frac{1}{\tau_{\rm opt}}=\frac{9D^2d_0^2m^2L}{4\pi^2B^2\rho\omega a_0^2\hbar^4}\Phi_{\rm op}(k_LL)\times\frac{E+\hbar\omega+(E-\hbar\omega)\theta(E-\hbar\omega)e^{\hbar\omega/k_BT}}{e^{\hbar\omega/k_BT}-1}\ . \tag{60}$$

For comparison we write down the relaxation rate without any selection rule with the coupling Hamiltonian $\mathcal{H}=d_ju_j/a_0$ and $d_j^2=d_0^2$ in the quantum well,

$$\frac{1}{\tau_{\rm opt}}=\frac{3d_0^2m}{\rho\hbar^2\omega La_0^2}\frac{1+\theta(E-\hbar\omega)e^{\hbar\omega/k_BT}}{e^{\hbar\omega/k_BT}-1}\ , \tag{61}$$

and in the bulk,[40]

$$\frac{1}{\tau_{\rm opt}}=\frac{d_0^2mk}{2\pi\rho\hbar^2\omega a_0^2}\frac{1+\theta(E-\hbar\omega)e^{\hbar\omega/k_BT}}{e^{\hbar\omega/k_BT}-1}\ . \tag{62}$$

Equations (60) and (61) differ by the dependence on the energy and the width of the well. Compared to Eq. (61), Eq. (62) contains the factor kL, similar to the case for acoustic phonons.[42,43]

F. Alloy-assisted optical-phonon scattering

Due to a specific symmetry, the deformation potential for optical-phonon scattering in the quantum well is reduced. As a result, this scattering can compete with any mechanism which lifts the symmetry and allows optical-phonon scattering, even with the wave functions in zero approximation, when only $\psi_{e1}(z)$ and $\psi_{o4}(z)$ are taken into account. In an alloy, the symmetry limitation is lifted by a random distribution of alloy atoms. Each unit cell containing different alloy atoms couples holes with optical phonons. The Hamiltonian describing this coupling can be written down in the form

$$\mathcal{H}_{\text{al-opt}}=\sum_{\alpha,\beta}d^j_{\alpha\beta}(\mathbf{r})u_j(\mathbf{r})\ , \tag{63}$$

where the average value of the random coupling function $d^j_{\alpha\beta}(\mathbf{r})$ is zero and its correlation function

$$\langle d^j_{\alpha\beta}(\mathbf{r})d^{j'}_{\alpha\beta}(\mathbf{r}')\rangle=x(1-x)d_1^2a_0\delta_{jj'}\delta_{\alpha\beta}\delta(\mathbf{r}-\mathbf{r}')\ . \tag{64}$$

Due to the short-range correlation the matrix element for this scattering mechanism does not depend on the transferred wave vector and all phonons in the Brillouin zone participate in the scattering. Calculations similar to those in the 3D case (see Ref. 40) lead to the following expression for the relaxation rate in a nondegenerate 2D hole gas:

$$\frac{1}{\tau_{\text{al-opt}}}=\frac{9d_1^2mx(1-x)}{4\rho\hbar^2\omega a_0^2L}\frac{1+\theta(E-\hbar\omega)e^{\hbar\omega/k_BT}}{e^{\hbar\omega/k_BT}-1}\ . \tag{65}$$

IV. SCATTERING RESULTING FROM COMPOSITIONAL FLUCTUATIONS

The scattering mechanisms considered in Sec. III assume that the material is a uniform medium described by a number of effective constants which are dependent on the composition. The only scattering associated with the distribution of Si and Ge atoms was the usual alloy disorder scattering due to a random distribution of these atoms. In this scattering an alien atom is considered as a short-range potential well. Meanwhile, in a real material a correlation of alloy atoms is possible, which can change this result or lead to other stronger effects. Correlation in the positions of alloy atoms, usually called clustering, was experimentally detected in $Al_yGa_{1-y}As$ alloys.[44,45] The effect of clustering of alloy atoms on mobility was discussed by Asch and Hall[46] and Ichimura and Sasaki,[47] and long-range earlier density fluctuations were considered by Brews.[48]

Schlimak, Efros, and Yanchev used a correlation between alloy atoms to explain their mobility data in bulk SiGe alloys.[49] They considered small clusters and the calculated mobility depended only on the average number of atoms in a cluster. Marsh modeled clusters in bulk $In_xGa_{1-x}As$ by spherically symmetric wells.[50] Ohno *et al.* used a Gaussian correlation function of alloy atoms for the explanation of the mobility data in $Al_yGa_{1-y}As/Ga_{1-x}In_xAs/GaAs$ heterostructures.[51]

In all of the above models clustering only modified the scattering by one alloy atom. At the same time clustering can lead to other stronger effects which are not described by the scattering in the Born approximation. Unfortunately, an adequate theoretical description of strong scattering in a random medium does not yet exist, and in this section we limit ourselves to some speculations and qualitative estimates. We specifically discuss scattering mechanisms resulting from localization of holes and nonuniform strain created by alloy atoms.

A. Scattering by localized holes

Compositional fluctuations or the clustering of alloy atoms leads to the existence of regions with variations in the position of the top of the valence band. The regions with a higher Ge concentration form wells for holes in a 2D gas. Quantum-mechanical calculations show that any small potential well binds a particle in a 2D gas. However, in a very narrow well the binding energy is exponentially small.[52] Thus, this energy can be smaller than the thermal energy or the energy uncertainty due to scattering, and one hardly should expect a bound state at each Ge atom. Clusters, however, can form a well in which holes can actually be localized. Such localized holes act to scatter other holes, thereby participating in conduction like charged impurities. In such a case the effective ionized impurity concentration that controls transport

can strongly exceed the actual concentration of background impurities in the sample.

B. Strain fluctuations

Another important result of compositional fluctuations is a nonuniform strain. The possible importance of strain fluctuations in a bulk SiGe alloy was shown by Raikh and Efros.[53] Lyo and Fritz explained electron mobility data in an $In_xGa_{1-x}As$ quantum well assuming strain fluctuations due to randomly distributed In atoms.[54] Here we estimate the effect of nonuniform strain resulting from compositional fluctuations in a SiGe quantum well.

We consider a model of a SiGe layer consisting of regions with two different Ge concentrations x_1 and x_2. These regions are taken to be distributed with the probabilities p_1 and p_2, respectively, where $p_1+p_2=1$. The equilibrium lattice constant of the material with a Ge concentration x_k is

$$a_k=a_{\rm Si}(1-x_k)+a_{\rm Ge}x_k=a_{\rm Si}(1-\alpha x_k) , \tag{66}$$

where $\alpha=a_{\rm Ge}/a_{\rm Si}-1=0.041$. The actual lattice constant in the lateral direction is controlled by the Si substrate. This results in the strain tensor components

$$\epsilon_{xx}=\epsilon_{yy}=\frac{a_k-a_{\rm Si}}{a_{\rm Si}} . \tag{67}$$

In the growth of the layer the average stress normal to the growth interface is zero. That is, the actual lattice constant in the z direction $\bar{a}$ can be found from the condition

$$p_1\sigma_{zz}^{(1)}+p_2\sigma_{zz}^{(2)}=0 . \tag{68}$$

The components of the stress tensor are expressed in terms of strain $\sigma_{zz}^{k}=c_{11}\epsilon_{zz}^{(k)}+c_{12}(\epsilon_{xx}^{(k)}+\epsilon_{yy}^{(k)})$, where c_{11} and c_{12} are elastic constants. Then

$$\bar{a}=p_1a_1+p_2a_2+2\frac{c_{12}}{c_{11}}[p_1(a_1-a_{\rm Si})+p_2(a_2-a_{\rm Si})] . \tag{69}$$

For the normal components of the strain tensor $\epsilon_{zz}^{(k)}=(a_k-\bar{a})/a_{\rm Si}$ we obtain the following expressions:

$$\epsilon_{zz}^{(1)}=p_2\frac{a_1-a_2}{a_{\rm Si}}-2\frac{c_{12}}{c_{11}}\left[p_1\frac{a_1-a_{\rm Si}}{a_{\rm Si}}+p_2\frac{a_2-a_{\rm Si}}{a_{\rm Si}}\right] , \tag{70}$$

$$\epsilon_{zz}^{(2)}=p_1\frac{a_2-a_1}{a_{\rm Si}}-2\frac{c_{12}}{c_{11}}\left[p_1\frac{a_1-a_{\rm Si}}{a_{\rm Si}}+p_2\frac{a_2-a_{\rm Si}}{a_{\rm Si}}\right] . \tag{71}$$

Equations (66), (67), (70), and (71) give the same uniaxial strain

$$\Delta\epsilon\equiv\epsilon_{xx}+\epsilon_{yy}-2\epsilon_{zz}=2\alpha\left[1+2\frac{c_{12}}{c_{11}}\right]\bar{x} , \tag{72}$$

where $\bar{x}=p_1x_1+p_2x_2$ is the average Ge concentration. The hydrostatic strain $\epsilon\equiv\epsilon_{xx}+\epsilon_{yy}+\epsilon_{zz}$ is different in different regions and the difference is

$$\epsilon^{(1)}-\epsilon^{(2)}=3\alpha(x_1-x_2) . \tag{73}$$

The relative shift of the top of the valence band in different regions

$$\Delta E=a(\epsilon^{(1)}-\epsilon^{(2)})=3a\alpha(x_1-x_2) . \tag{74}$$

The hydrostatic deformation potential in both Si and Ge is about 11 eV (Table I). Using this value we obtain a ΔE of about 13 meV for a Ge concentration fluctuation of 1%. This value equals or even exceeds the typical Fermi energy in the 2D gas. Hence, very small compositional fluctuations can induce huge fluctuations in the top of the valence band. Such fluctuations lead to a very strong scattering. Essentially, the mean free path in this case is of the order of the correlation length of the fluctuations.

The model is too simplified to describe all the strain effects resulting from the compositional fluctuations. Even in the case of two kinds of regions with different Ge concentrations, there are strains near the boundaries of the regions which violate the symmetry of the problem. The order of magnitude of these strains may be smaller than those estimated above. Nevertheless, the symmetry violation leads to a change of the band structure which can result in two important effects. The first is the change of the effective mass and the second is the split of the doubly degenerate HH1 level. The estimate of these effects, however, is beyond the scope of the present work.

V. NUMERICAL RESULTS ON THE MOBILITY

For the numerical calculations of the mobility, we will focus on a 60-Å well with a Ge content of 40%, which represents a case where the ground-state mass is light and the subband splitting is several kT at room temperature. Specifically, the calculated HH1 effective mass and the HH1-HH2 subband splitting are 0.12 and 125 meV, respectively, for this structure. We assume a 2D hole gas density of 10^{12} cm^{-2}. Ohter parameters used in the calculations are given in Table I.

In the acoustic-phonon scattering, we neglect the uniaxial deformation potential b compared to the hydrostatic potential a. Parameters for $Si_{1-x}Ge_x$ alloys are obtained by linear interpolation. The optical-phonon energies are very different in Si and Ge, so we interpolate the inverse relaxation times for optical-phonon scattering. For alloy-assisted optical-phonon scattering, however, the interpolated optical-phonon energy is used. Where parameters are not available in the literature, roughly estimated values based on reasonable limits are used. Specifically, the deformation potential for alloy-assisted optical-phonon scattering d_1 is taken to be 30 eV and the scattering potential of alloy atoms $u_{\rm al}$ is taken to be 0.3 eV. The former value is taken to be of the order of the optical-phonon deformation potential. For the latter parameter, one good estimate may be the Si/Ge band offset 0.74 eV (compare Ref. 37). One impurity atom is, however, not enough to completely create the different band structure, and for the scattering potential we used a

smaller value. In the following, we show results separately for the various scattering mechanisms over ranges in temperature and other relevant parameters.

The impurity-scattering mobility is shown in Fig. 4 for different levels of the background impurity density. For the background impurity density expected in high-quality SiGe layers less than 10^{16} cm^{-3}, the mobility is extremely high, over 10^5 cm^2/V s. For layers doped at a level of 10^{18} cm^{-3}, as would be encountered in a doped-channel FET structure, we still see reasonably good mobilities of 4000 cm^2/V s at room temperature and about 2000 cm^2/V s at low temperatures. For a level of 10^{19} cm^{-3}, however, the mobility drops to a low level of several hundred cm^2/V s. These values of mobility are nearly 10 times higher than for comparably doped bulk Si.[55] This is advantageous for doped-channel structures. The temperature dependence in Fig. 4 is weak compared to that for doped bulk material due to the fact that the 2D hole gas in the quantum well is degenerate in all cases for the assumed 10^{12} cm^{-2} density.

The interface-roughness mobility in the 60-Å, 40% quantum well is shown as a function of the correlation length Λ in Fig. 5. The average height of the roughness Δ is assumed to be 5 Å. This value of Δ corresponds to approximately a 14-Å peak to valley distance and, hence, would represent a very rough interface for a 60-Å SiGe layer. It can be seen that the mobility has a pronounced minimum at a correlation length in the range of 20 to 50 Å, depending on temperature. The minimum mobility increases by about a factor of 2 as the temperature is increased. For the roughness parameters used in this figure, high mobilities of over 10^4 are obtained even for the worst case. The sensitivity of the mobility to Ge content is weak and is mainly related to the dependence on effective mass.

Within the present model, the mobility for other levels of roughness may be determined by scaling the mobility data, which goes as Δ^{-2}. The dependence of the interface-roughness mobility on the quantum-well width

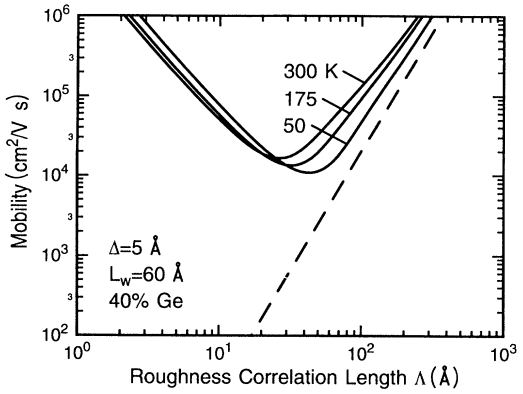

FIG. 5. Interface-roughness limited mobility as a function of the correlation length Λ. The dashed line corresponds to the asymptotic expression in Eq. (28).

is shown in Fig. 6. Here we have assumed a temperature of 100 K and a correlation length of 30 Å, which represents a worst case. The mobility follows an L^6 dependence, reaching a level of 1250 cm^2/V s at a width of 40 Å.

The calculated mobilities for various lattice-scattering mechanisms and alloy disorder scattering are shown as a function of temperature in Fig. 7. Results are shown for acoustic-mode scattering, optical-mode scattering, alloy-assisted optical-mode scattering, and alloy scattering in a 60-Å well with 40% Ge. It can be seen that the mobility is limited to a level of about 5×10^3 cm^2/V s at room temperature due to a combination of acoustic-phonon and alloy scattering in the well. Acoustic-phonon scattering dominates at room temperature, as in the bulk case. Alloy scattering limits the mobility in Fig. 7 to 3×10^4 cm^2/V s at low temperatures. Unfortunately, the accuracy of this estimate is uncertain at present due to the lack of data on the alloy scattering potential. An accurate determination of this parameter is needed for a quantita-

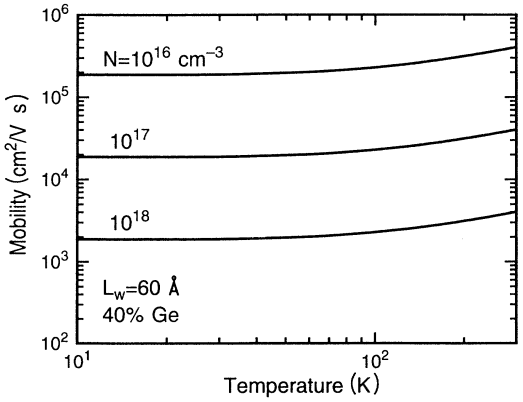

FIG. 4. Mobility limited by ionized-impurity scattering within the well. At low temperature the value of the mobility is about five times smaller than that for the conduction band (Ref. 31).

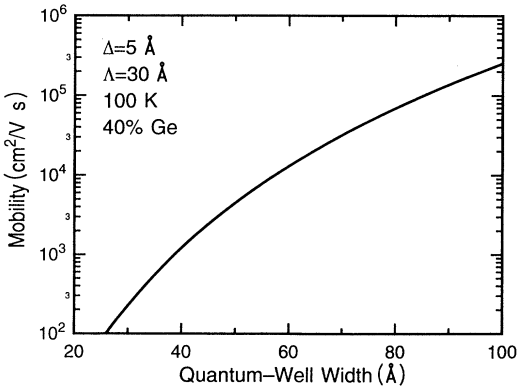

FIG. 6. Interface-roughness limited mobility as a function of the width of the well.

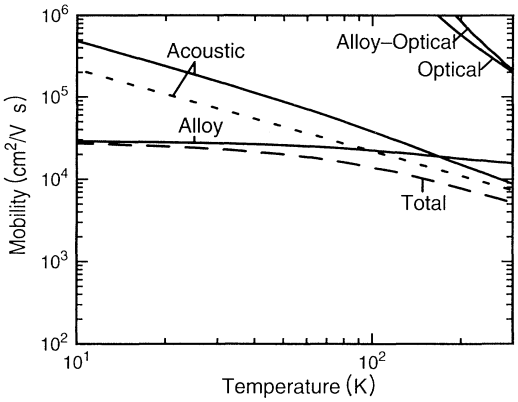

FIG. 7. Temperature dependence of mobility limited by optical-phonon, alloy-assisted optical phonon, acoustic-phonon, and alloy scattering. The dotted curve corresponds to the asymptotic expression for acoustic-phonon limited mobility given in Eq. (49).

tive estimate of the low-temperature mobility in these structures.

Figure 7 also indicates that optical-phonon and alloy-assisted optical-phonon scattering are both very weak in a narrow well. Compared with other scattering mechanisms, scattering with optical phonons is weakened the most because of the selection rule for intrasubband scattering and the lack of intersubband scattering in a narrow quantum well with a large subband separation. We mention that although the deformation potential for alloy-assisted optical-mode scattering only has been roughly estimated, it appears quite unlikely that this mechanism could play a dominant role in determining the mobility since its estimated value is so small.

The phonon-limited mobilities for the narrow SiGe quantum well in Fig. 7 are substantially greater than the phonon-limited hole mobilities in bulk Si (viz., 400 and 8000 $cm^2/V\,s$ at 300 and 77 K, respectively[28]). One can expect the quantum-well values to approach those in bulk material with increases in the width of the well such that the subband separation is reduced and the occupation of higher subbands and intersubband scattering becomes appreciable. In this case it is necessary to take into account the nonparabolicity of the HH1 subband. In such a wide well the hole effective mass is determined by a region of large $k_{\|}$ and the parabolic region near $k_{\|}=0$ is reduced and has little effect on the transport.[23] Calculations including these effects are beyond the scope of the present work.

Comparison of the results in Fig. 7 with the Monte Carlo calculations by Kelsall *et al.*[21] for a 90-Å $In_xGa_{1-x}As$ quantum well at 77 K shows the same range of values for the acoustic-phonon mobility and alloy scattering mobility in the two cases. A more detailed comparison is difficult to make since Kelsall *et al.* show only the final result of their calculation.

VI. CONCLUSIONS

The valence band in a narrow Si/SiGe quantum well with a high Ge content is characterized by a light mass over a very large range of wave vectors and by large subband separations. In particular, a 60-Å SiGe layer with a Ge content of 40% has a zone-center mass of 0.12 which remains light for wave vectors as large as 0.3 nm^{-2} and has a subband splitting of 125 meV. As a result, transport is expected to be dominated by a light mass for densities well above 10^{12} cm^{-2}, even at room temperature. In addition, scattering rates are expected to be reduced as a consequence of the light mass and large subband splittings, which greatly reduce the phase space for scattering.

Models for the scattering within a single parabolic band characterized by an isotropic light mass were used to determine the limitations imposed by various scattering mechanisms on the hole mobility in such structures. Optical-phonon scattering mechanisms were found to be very weak, primarily as a result of the elimination of intersubband scattering. Acoustic-phonon scattering was found to dominate the room-temperature mobility, as in the case of bulk material. However, acoustic-phonon mobility approaches a high value of 10^4 $cm^2/V\,s$ due to the light mass and the lack of intersubband scattering. Alloy scattering was found to dominate the low-temperature mobility, and a value of 3×10^4 $cm^2/V\,s$ was estimated for a 40% Ge layer. Impurity scattering in such structures is weaker than in bulk material and should not impact these mobilities for concentrations below 10^{17} cm^{-3}. Finally, an interface-roughness mobility of 10^4 $cm^2/V\,s$ was obtained for a 60-Å, 40% well with even a very rough interface ($\Delta=5$ Å and $\Lambda=30$ Å), and significant degradation from roughness is therefore expected only for wells less than 40 Å in thickness.

Our results show that narrow Si/SiGe quantum wells could provide very high hole mobilities in the mid 10^3 $cm^2/V\,s$ range at room temperature and mid 10^4 $cm^2/V\,s$ range at low temperatures. These values are about an order of magnitude higher than reported for Si/SiGe heterostructures thus far.[6,7] While further study is needed to determine whether other effects, such as scattering by compositional fluctuations, might seriously impact mobility, these results indicate that narrow Si/SiGe quantum wells with high Ge content could provide the basis for greatly improved *p*-channel MOSFET's.

ACKNOWLEDGMENTS

The authors are grateful to F. Stern and P. J. Price for many informative discussions.

*Present address: Fujitsu Laboratories Ltd., 10-1 Morinosato-Wakamiya, Atsugi 243-01, Japan.

[1]S. S. Iyer, P. M. Solomon, V. P. Kesan, A. A. Bright, J. L. Freeouf, T. N. Nguyen, and A. C. Warren, IEEE Electron Device Lett. **12**, 246 (1991).

[2]P. M. Garone, V. Venkataraman, and J. C. Sturm, IEEE Electron Device Lett. **12**, 230 (1991).

[3]D. K. Nayak, J. C. S. Woo, J. S. Park, K.-L. Wang, and K. P.

MacWilliams, IEEE Electron Device Lett. **12**, 154 (1991).
[4]J. M. Hinckley and J. Singh, Phys. Rev. B **41**, 2912 (1990).
[5]G. C. Osbourn, P. L. Bourley, I. J. Fritz, R. M. Biefield, L. R. Dawson, and T. E. Zipperian, in *Applications of Multiquantum Wells, Selective Doping, and Superlattices,* Vol. 24 of *Semiconductors and Semimetals,* edited by R. K. Willardson and A. C. Beer (Academic, New York, 1975).
[6]P. J. Wang, B. S. Meyerson, F. F. Fang, J. Nocera, and B. Parker, Appl. Phys. Lett. **55**, 2333 (1989).
[7]P. M. Garone, V. Venkataraman, and J. C. Sturm, IEEE Electron Device Lett. **13**, 56 (1992).
[8]S. Verdonckt-Vandebroek, E. F. Crabbe, B. S. Meyerson, D. L. Harame, P. J. Restle, J. M. C. Stork, A. C. Meganis, C. L. Stanis, A. A. Bright, G. M. W. Kroesen, and A. C. Warren (unpublished).
[9]V. P. Kesan, S. Subbanna, T. J. Restle, M. J. Tejwani, J. M. Altken, S. S. Iyer, and J. A. Ott (unpublished).
[10]R. A. Kiehl, H. Shtrikman, and J. Yates, Appl. Phys. Lett. **58**, 954 (1991).
[11]B. Laikhtman, Appl. Phys. Lett. **59**, 3021 (1991).
[12]G. L. Bir and G. E. Pikus, *Symmetry and Strain-Induced Effects in Semiconductors* (Wiley, New York, 1974).
[13]J. D. Wiley, in *Transport Phenomena,* Vol. 10 of *Semiconductors and Semimetals,* edited by R. K. Willardson and A. C. Beer (Academic, New York, 1975).
[14]G. Ottaviani, L. Reggiani, C. Canali, F. Nava, and A. Alberigi-Quaranta, Phys. Rev. B **12**, 3318 (1975).
[15]H. Nakagawa and S. Zukotynski, Can. J. Phys. **55**, 1485 (1977).
[16]T. Manku and A. Nathan, IEEE Electron Device Lett. **12**, 704 (1991).
[17]S. Manzini and A. Modelli, J. Appl. Phys. **65**, 2361 (1988).
[18]M. Tiersten, J. Phys. Chem. Solids **25**, 1151 (1968).
[19]F. Szmulowicz, Phys. Rev. B **28**, 5943 (1983).
[20]R. W. Kelsall, R. I. Taylor, A. C. G. Wood, and R. A. Abram, Semicond. Sci. Technol. **5**, 877 (1990).
[21]R. W. Kelsall, R. A. Abram, W. Batty, and E. P. O'Reilly, Semicond. Sci. Technol. **7**, 86 (1992).
[22]A. Gold, Phys. Rev. B **35**, 723 (1987).
[23]B. Laikhtman, R. A. Kiehl, and D. J. Frank, J. Appl. Phys. **70**, 1531 (1991); **70**, 5719 (1991).
[24]C. G. Van de Walle and R. M. Martin, Phys. Rev. B **34**, 5261 (1986).
[25]R. People and J. C. Bean, Appl. Phys. Lett. **48**, 538 (1986).
[26]W.-X. Ni and G. V. Hansson, Phys. Rev. B **42**, 3030 (1990).
[27]B. Laikhtman, Phys. Rev. B **46**, 4769 (1992).
[28]*Numerical Data and Functional Relationships in Science and Technology,* Landolt-Bornstein, Group III, New Series, Vol. 17, Pt. a (Springer-Verlag, New York, 1982); *ibid.* Vol. 22, Pt. a (Springer-Verlag, New York, 1987).
[29]G. A. Vawter and D. R. Myers, J. Appl. Phys. **65**, 4769 (1989).
[30]T. Ando, A. B. Fowler, and F. Stern, Rev. Mod. Phys. **54**, 437 (1982).
[31]A. Gold and V. T. Dolgopolov, Phys. Rev. B **33**, 1076 (1986).
[32]P. F. Maldague, Surf. Sci. **73**, 296 (1978).
[33]A. Gold, Solid State Commun. **60**, 531 (1986).
[34]H. Sakaki, T. Noda, K. Hirakawa, M. Tanaka, and T. Matsusue, Appl. Phys. Lett. **51**, 1934 (1987).
[35]R. Gottinger, A. Gold, G. Abstreiter, G. Weimann, and W. Schlapp, Europhys. Lett. **6**, 183 (1988).
[36]J. C. Hensel and G. Feher, Phys. Rev. **129**, 1041 (1963).
[37]T. Ando, J. Phys. Soc. Jpn. **51**, 3900 (1982).
[38]G. Bastard, Appl. Phys. Lett. **43**, 591 (1983).
[39]A. Gold, Phys. Rev. B **38**, 10798 (1988).
[40]B. R. Nag, *Theory of Electrical Transport in Semiconductors* (Pergamon, Oxford, 1972), pp. 110 and 111.
[41]V. F. Gantmakher and Y. B. Levinson, *Carrier Scattering in Metals and Semiconductors* (North-Holland, New York, 1987), pp. 89–100.
[42]S. Kawaji, J. Phys. Soc. Jpn. **27**, 906 (1969).
[43]P. J. Price, Ann. Phys. **133**, 217 (1981).
[44]N. Holonyak, Jr., W. D. Laidig, B. A. Vojak, K. Hess, J. J. Coleman, P. D. Dapkus, and J. Bardeen, Phys. Rev. Lett. **45**, 1703 (1980); N. Holonyak, Jr., W. D. Laidig, K. Hess, J. J. Coleman, and P. D. Dapkus, *ibid.* **46**, 1043 (1981); N. Holonyak, Jr., W. D. Laidig, M. D. Camras, H. Morkoc, T. J. Drummond, K. Hess, and M. S. Burroughs, J. Appl. Phys. **52**, 7201 (1981).
[45]M. S. Burroughs, K. Hess, N. Holonyak, Jr., W. D. Laidig, and G. E. Stillman, Solid State Electron. **25**, 161 (1982).
[46]A. E. Asch and G. L. Hall, Phys. Rev. **132**, 1047 (1963).
[47]M. Ichimura and A. Sasaki, Jpn. J. Appl. Phys. **26**, 776 (1987).
[48]J. R. Brews, J. Appl. Phys. **46**, 2181 (1975); **46**, 2193 (1975).
[49]I. S. Schlimak, A. L. Efros, and I. Ya. Yanchev, Fiz. Tekh. Poluprovodn. **11**, 149 (1977) [Sov. Phys. Semicond. **11**, 149 (1977)].
[50]J. H. Marsh, Appl. Phys. Lett. **41**, 732 (1982).
[51]H. Ohno, J. K. Luo, K. Matsuzaki, and H. Hasegawa, Appl. Phys. Lett. **54**, 36 (1988).
[52]L. D. Landau and E. M. Lifshitz, *Quantum Mechanics: Nonrelativistic Theory* (Pergamon, Oxford, 1977).
[53]N. E. Raikh and A. L. Efros, Fiz. Tverd. Tela (Leningrad) **26**, 1508 (1984) [Sov. Phys. Solid State **28**, 916 (1984)].
[54]S. K. Lyo and I. J. Fritz, Phys. Rev. B **46**, 7931 (1992).
[55]S. S. Li, Solid-State Electron. **21**, 1109 (1978).